



S. Toppaladoddi^{1,2}, W. Moon³ , and J. S. Wettlaufer^{4,5} 

¹University of Leeds, Leeds, UK, ²University of Oxford, Oxford, UK, ³Department of Environmental Atmospheric Sciences, Pukyong National University, Pusan, South Korea, ⁴Yale University, New Haven, CT, USA, ⁵Nordita, Royal Institute of Technology and Stockholm University, Stockholm, Sweden

Key Points:

- A new theory that accounts for the formation of open-water in the Arctic during spring and summer has been developed
- A second peak in the thickness distribution is observed to emerge in summer, in agreement with observations
- The ice cover becomes indistinguishable from open water when the ocean heat flux is 60 Wm^{-2}

Correspondence to:

J. S. Wettlaufer,
jw@fysik.su.se

Citation:

Toppaladoddi, S., Moon, W., & Wettlaufer, J. S. (2023). Seasonal evolution of the Arctic sea ice thickness distribution. *Journal of Geophysical Research: Oceans*, 128, e2022JC019540. <https://doi.org/10.1029/2022JC019540>

Received 2 DEC 2022
Accepted 15 MAY 2023

Abstract The Thorndike et al. (1975, <https://doi.org/10.1029/jc080i033p04501>) theory of the ice thickness distribution, $g(h)$, treats the dynamic and thermodynamic aggregate properties of the ice pack in a novel and physically self-consistent manner. Therefore, it has provided the conceptual basis of the treatment of sea-ice thickness categories in climate models. The approach, however, is not mathematically closed due to the treatment of mechanical deformation using the redistribution function ψ , the authors noting “The present theory suffers from a burdensome and arbitrary redistribution function ψ .” Toppaladoddi and Wettlaufer (2015, <https://doi.org/10.1103/physrevlett.115.148501>) showed how ψ can be written in terms of $g(h)$, thereby solving the mathematical closure problem and writing the theory in terms of a Fokker-Planck equation, which they solved analytically to quantitatively reproduce the observed winter $g(h)$. Here, we extend this approach to include open water by formulating a new boundary condition for their Fokker-Planck equation, which is then coupled to the observationally consistent sea-ice growth model of Semtner (1976, [https://doi.org/10.1175/1520-0485\(1976\)006<0379:amfttg>2.0.co;2](https://doi.org/10.1175/1520-0485(1976)006<0379:amfttg>2.0.co;2)) to study the seasonal evolution of $g(h)$. We find that as the ice thins, $g(h)$ transitions from a single- to a double-peaked distribution, which is in agreement with observations. To understand the cause of this transition, we construct a simpler description of the system using the equivalent Langevin equation formulation and solve the resulting stochastic ordinary differential equation numerically. Finally, we solve the Fokker-Planck equation for $g(h)$ under different climatological conditions to study the evolution of the open-water fraction.

Plain Language Summary A quantitative understanding of the evolution of the thickness distribution of sea ice is necessary to accurately predict changes in the Arctic ice cover. In the original formulation of the governing equation for the thickness distribution by Thorndike et al., the treatment of the redistribution term—which represents the mechanical deformation of ice by rafting and ridging—is referred to as “arbitrary” and “burdensome.” Using an analogy with Brownian motion, we have recast the redistribution term, closed the original theory and incorporated the process of open water formation to produce seasonal predictions of the thickness distribution. Using our theory we show that a second peak in the thickness distribution emerges in summer, which is consistent with observations. Furthermore, we explore how the greenhouse gas and oceanic heat flux forcings impact the open-water fraction and mean thickness, and the relative sensitivities to these forcings.

1. Introduction

Arctic sea ice is one of the most important components of the Earth's climate system. Its importance stems primarily from the role it plays in influencing Earth's radiation budget through its albedo and in driving the thermohaline circulation (Kwok & Untersteiner, 2011). Any climatological study of Arctic sea ice necessarily involves the evolution of the sea-ice volume and its interactions with the other components of the climate system. Although routine measurement of the areal extent of sea ice using satellites is now possible, a routine measurement of its thickness still remains challenging (Kwok et al., 2021). This motivates the development of an observationally consistent mathematical theory to study the evolution of the thickness field.

The sea-ice cover consists of a complex discontinuous mosaic of floes of varying size and thickness (Rothrock & Thorndike, 1980, 1984), which makes any deterministic description of the system on a geophysical scale extremely difficult. The first General Circulation Models (GCM) computed the full three-dimensional fluid dynamical and radiative-thermodynamical transport equations around an idealized globe (Manabe & Wetherald, 1975). However, their treatment of sea ice was simply as a thermal boundary condition on the ocean (Manabe & Wetherald, 1975), and hence did not capture the fact that pack ice consists of a multi-scale aggregate

© 2023. The Authors.

This is an open access article under the terms of the [Creative Commons Attribution License](https://creativecommons.org/licenses/by/4.0/), which permits use, distribution and reproduction in any medium, provided the original work is properly cited.

of individual ice floes that evolve dynamically and thermodynamically. Contemporaneously, this reality was the focus of the multi-year Arctic Ice Dynamics Joint Experiment (AIDJEX), which began in 1970 and culminated with the main field experiment from March 1975 to May 1976 (Untersteiner et al., 2007). In the same spirit as the GCMs the AIDJEX model treated sea ice in the spirit of weather forecasting; solving the appropriate conservation laws on a ~ 100 km scale. The momentum equation for the ice pack includes the tangential wind and ocean stresses, the Coriolis effect, and the dynamic tilt of the sea surface. Counteracting these external forces is the internal stress with which the ice pack resists deformation, parameterized by a “constitutive law” relating the internal stress to the deformation rate. Whilst the floe-scale processes responsible for the deformation of the ice pack, and the resulting floe-size and thickness distribution, may be the foundation for the constitutive behavior, we still lack a constitutive law. Indeed, the state of affairs during AIDJEX, as expressed by Rothrock (1975):

“If we knew what the constitutive equation for pack ice should be, we would not need to pay attention to the mechanisms of floe interaction. But the simple fact is that we are not at all sure about the constitutive equation...we have turned to the study of these mechanisms—rafting, ridging, shearing, and opening—to deduce what we can about the large-scale mechanical behavior of pack ice.”

has not changed. Moreover, despite having since derived a quantitative treatment of rafting and ridging (Vella & Wettlaufer, 2008), translating these into any constitutive law for the ice pack still poses an outstanding challenge for any continuum momentum equation that is not scale-dependent and/or highly parameterized for inclusion in climate models (Coon et al., 2007; Feltham, 2008; Roberts et al., 2019; Untersteiner et al., 2007).

Within the AIDJEX modeling group an approach that abandons the explicit use of a momentum equation was developed by Thorndike et al. (1975). They considered the corpus of mechanical, dynamical and thermodynamical effects in a region of the ice pack with area \mathcal{R} , which give rise to the sea-ice thickness distribution, $g(h)$, defined as

$$\int_{h_1}^{h_2} g(h) dh = \frac{R}{\mathcal{R}}, \quad (1)$$

where h is the ice thickness and $R(\leq \mathcal{R})$ is the area within \mathcal{R} that contains ice between thicknesses h_1 and h_2 . Defined this way, $g(h)$ is the probability density function (PDF) for h . Their evolution equation for $g(h)$ is (Thorndike et al., 1975)

$$\frac{\partial g}{\partial t} = -\nabla \cdot (\mathbf{u} g) - \frac{\partial}{\partial h}(f g) + \psi. \quad (2)$$

Here, \mathbf{u} is the horizontal velocity of the ice pack, f is thermodynamic growth-rate of ice, and ψ represents the mechanical interactions between ice floes. Note that in general the ice grows and decays and the distribution evolves under deformation and hence $g = g(h(t), t)$. However, unless making an explicit point about this time dependence, for compactness we write $g = g(h)$, or simply g .

Although the concept of the ice thickness distribution has been used as an organizing principle for the categories of ice produced in momentum equation based climate models, it has not been an explicit prognostic variable, which was the original intent (Thorndike et al., 1975). The principal difficulty in solving Equation 2 is associated with ψ , which translates the intransigence of the constitutive law problem in the momentum equation approach to the mechanical deformation in the theory for $g(h)$. Studies have been devoted to constructing simplified descriptions of ψ (Godlovitch et al., 2011; Thorndike, 1992, 2000; Thorndike et al., 1975), but the results are either valid for only steady state or capture only the thick end of the distribution. Other approaches recast the redistribution function of Thorndike et al. (1975) in different notation (Horvat & Tziperman, 2015). A more detailed discussion of these studies can be found in Toppaladoddi and Wettlaufer (2017).

In order to close Equation 2 in a mathematically consistent manner, one must write ψ in terms of $g(h)$. This is done by recognizing that there is a vast separation of time and length scales between the individual mechanical interactions that change the ice thickness and the confluence of processes that change the large-scale evolution of $g(h)$ (Toppaladoddi & Wettlaufer, 2015, 2017). This naturally leads to an analogy with Brownian motion, wherein there is a vast gulf between the time scales of individual collisions of solvent molecules with a pollen grain and the

overall displacement of the latter. To wit, Toppaladoddi and Wettlaufer (Toppaladoddi & Wettlaufer, 2015, 2017) interpreted ψ as a collision integral:

$$\psi(h, t) = \int_0^\infty [g(h', t) w(h, h') - g(h, t) w(h', h)] dh', \quad (3)$$

in which, $w(h, h')$ and $w(h', h)$ are the transition probabilities per unit time that represent deformation processes changing ice thickness from h' to h and from h to h' , respectively. Assuming $w(h, h') = w(h', h)$, which implies that the transition density depends only on the difference of the thicknesses of the participating ice floes, then the Kramers-Moyal-Taylor expansion of Equation 3 transforms Equation 2 into

$$\frac{\partial g}{\partial t} = -\nabla \cdot (\mathbf{u} g) - \frac{\partial}{\partial h} (f g) + \frac{\partial}{\partial h} (k_1 g) + \frac{\partial^2}{\partial h^2} (k_2 g), \quad (4)$$

where

$$k_1 = \int_0^\infty |h' - h| w(h, h') dh' \quad (5)$$

and

$$k_2 = \int_0^\infty \frac{1}{2} |h' - h|^2 w(h, h') dh' \quad (6)$$

are the first and second moments over the transition density (Toppaladoddi & Wettlaufer, 2015, 2017). The Pawula theorem (Pawula, 1967) guarantees that Equation 4 is well-posed in the sense of Hadamard, and hence obeys a maximum principle (Courant & Hilbert, 1953), insuring that $g(h)$ is a well defined PDF. Moreover, assuming that the first and second moments over the transition probabilities are constant in the region \mathcal{R} is equivalent to the assumption that the physics of ice deformation is the same anywhere within it. For example, ice ridging is governed by the same basic physical processes anywhere in the ice pack (Rothrock, 1975; Vella & Wettlaufer, 2008).

Equation 4 can be non-dimensionalized using H_{eq} , the seasonal mean ice thickness, as the vertical length scale; L as the horizontal length scale; U_0 as the velocity scale for the horizontal ice velocity; $t_m = L/U_0$ as the time scale for advection of ice floes; $t_D = H_{eq}^2/\kappa$, where κ is the thermal diffusivity of ice, as the diffusion time scale; and $t_R \sim 1/\dot{\gamma}$, where $\dot{\gamma}$ is the collisional strain rate, as the relaxation time scale. Because the deformation in the ice pack is driven by the wind, we have $t_m \approx t_R$. The remaining terms have the following scalings: $f_0 = H_{eq}/t_D$, $\tilde{k}_1 = H_{eq}/t_R$, and $\tilde{k}_2 = H_{eq}^2/t_R$. Finally, observations in the central Arctic spanning 1978–2015 show that the mean divergence field is solenoidal to a part in 10^{11} (Agarwal & Wettlaufer, 2017). Thus, we follow \mathcal{R} in the Lagrangian frame, and retaining the pre-scaled notation, Equation 4 becomes

$$\frac{Dg}{Dt} = \frac{\partial}{\partial h} [(k_1 - \tau f)g] + \frac{\partial^2}{\partial h^2} (k_2 g) = -\frac{\partial J}{\partial h}, \quad (7)$$

where $\tau \equiv t_m/t_D \ll 1$ where

$$J = -\left[(k_1 - \tau f)g + k_2 \frac{\partial g}{\partial h} \right] \quad (8)$$

is the total flux of probability. This closes the theory of Thorndike et al. (1975), which we have transformed into a Fokker-Planck Equation.

During winter, open water rapidly freezes. Hence, Toppaladoddi and Wettlaufer (2015) used the boundary conditions $g(h=0) = g(h=\infty) = 0$ to study the winter ice pack. They found that the winter season is governed by the following invariant measure of Equation 7,

$$g(h) = \mathcal{N}(q) h^q e^{-h/H}, \quad (9)$$

with prefactor $\mathcal{N}(q) = [H^{1+q}\Gamma(1+q)]^{-1}$, wherein $\Gamma(x)$ is the Euler gamma function, as determined by the normalization condition $\int_0^\infty g(h)dh = 1$. Hence, $\mathcal{N}(q)$ is unique and single valued for $\mathbb{R}(q) > -1$ and $\mathbb{R}(H) > 0$.

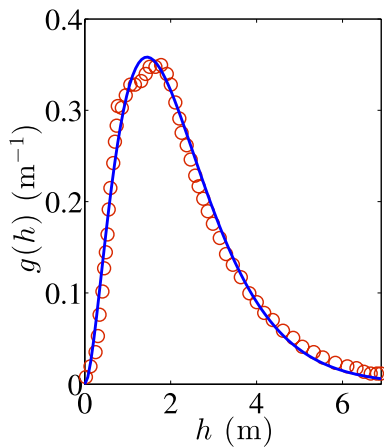


Figure 1. Comparison of the steady solution to Equations 7 and 8 (lines), with satellite measurements from ICESat (Kwok et al., 2009), for February through March of 2008 (circles) from Toppaladoddi and Wettlaufer (2015). The two parameters from Equation 9 are $q = 1.849$ and $H = 0.783$ m. The constants k_1 and k_2 are obtained using these values of q and H .

Here, $q = \tau c_p \Delta T / k_2 L_i$ and $H = k_2 / k_1$, where L_i , c_p and ΔT are the latent heat of fusion of ice, the specific heat of ice at constant pressure and the temperature difference across the ice layer, respectively. The dimensionless thermodynamic ice growth rate is $f = c_p \Delta T / L_i h \equiv 1 / Sh$, where $S = L_i / c_p \Delta T$ is the Stefan number and k_2 represents mechanical deformation, so that q characterizes the combined effects of both processes, whereas H is solely associated with mechanical deformation. Importantly, q and H are the sole parameters associated with the bivariate satellite observations for the winter months (Kwok & Cunningham, 2015; Kwok et al., 2009) as reproduced here in Figure 1. Thus, for $h \ll 1$, $g(h)$ is controlled by both thermodynamics and mechanics, whereas for $h \gg 1$, $g(h)$ is controlled solely by mechanical interactions, showing that the thick end of the distribution can only be achieved by ice deformation. The dimensionless constants k_1 and k_2 are obtained using:

$$q = \frac{\epsilon}{k_2} \text{ and } H = \frac{k_2}{k_1},$$

where $\epsilon = \tau / S$. The parameters q and H are obtained from the fit of the functional form of the solution (Equation 9) to satellite observations from ICESat (see Figure 1). We estimate $\tau \approx 0.46$ and $S \approx 10$, giving $\epsilon \approx 0.046$, and using $H_{eq} = 1.5$ m, we get $k_1 = 0.048$ and $k_2 = 0.025$. These are the values used in this study.

We note that the condition $g(h = 0) = 0$ implies that there is no open water in the study region \mathcal{R} . As shown in Figure 1, this is a reasonable approximation in winter, when the open water rapidly freezes and on average only a small fraction of the distribution neglected. However, this is not the case for the full seasonal cycle. Indeed, a particular challenge in formulating a boundary condition for $g(h)$ at $h = 0$ is that open water forms through both thermodynamic and mechanical processes. Thus, $g(h = 0)$ must be obtained as a part of the solution to Equation 7. Therefore, we formulate a complete seasonal boundary condition for $g(h)$ at $h = 0$ and study the evolution of $g(h)$ with the aide of the one-dimensional sea-ice growth model of Semtner (1976) in Equation 7.

2. The Open Water Fraction

Let A be the fraction of open water present in the region \mathcal{R} . The normalization condition for $g(h)$ is then

$$A + \int_{0^+}^{\infty} g(h, t) dh = 1. \quad (10)$$

Differentiating this with respect to t gives

$$\frac{dA}{dt} = - \int_{0^+}^{\infty} \frac{Dg(h, t)}{Dt} dh, \quad (11)$$

and using Equation 7 in Equation 11 yields

$$\frac{dA}{dt} = [J|_{h=\infty} - J|_{h=0^+}] = -J|_{h=0^+}. \quad (12)$$

Therefore, as is observed, A increases (decreases) as the Arctic enters spring and summer (fall and winter) during which $J|_{h=0^+} \leq 0$ ($J|_{h=0^+} \geq 0$).

In order to relate the open water fraction, $A(t)$, to the thickness distribution at the origin, $g(h = 0, t)$, we let:

$$A(t) \equiv g(0, t) H_c. \quad (13)$$

In dimensional terms $\tilde{H}_c \equiv \zeta \Lambda$, where ζ is the fraction of the spectrally and angularly averaged Beer's extinction length, Λ , below which thin ice and open water become indistinguishable. Taking ζ to be 15% of the extinction length appropriate for H_{eq} , which is $\Lambda = 67$ cm (Maykut & Untersteiner, 1971), gives $\tilde{H}_c = 10$ cm. Using this in Equation 12 gives

$$\frac{dg(0, t)}{dt} = -\frac{1}{H_c} J|_{h=0^+}, \quad (14)$$

which is the required evolution equation for $g(0, t)$. Equation 7, along with the boundary conditions (Equation 14) and $g(\infty) = 0$, can now be used to solve for $g(h, t)$. Once $g(h, t)$ is known, $A(t)$ can be calculated from Equation 10. We follow Toppaladoddi and Wettlaufer (2015) and impose $g(0, t) = 0$ during winter, and Equation 14 for the remaining part of the year. The transition between these boundary conditions is determined by the sign of the thermal growth rate of open water, $f(0, t)$, which is positive in winter.

3. Thermal Growth of Sea Ice

To calculate the thermal growth rate of sea ice, $f(h, t)$, we use the observationally consistent one-dimensional model by Semtner (1976). The thickness of the snow layer is assumed to be uniform across all the thicknesses and is prescribed following Maykut and Untersteiner (1971): 30 cm from August 20 to October 30, 5 cm from November 1 to April 30, and 5 cm during the month of May. Snow is taken to accumulate only when the mean surface temperature of the ice layer or the snow layer is below the freezing point, and the increase in the snow thickness is taken to be linear (Maykut & Untersteiner, 1971). The values of snow albedo for the different months are taken from Maykut and Untersteiner (1971), and the thickness-dependent albedo of sea ice is obtained using the expression from Eisenman and Wettlaufer (2009):

$$\alpha(h) = \left(\frac{\alpha_w + \alpha_i}{2}\right) + \left(\frac{\alpha_w - \alpha_i}{2}\right) \tanh\left(-\frac{h}{\Lambda}\right), \quad (15)$$

where α_w and α_i are the albedos of open water and the thickest ice, respectively, and as discussed above Λ is the Beer's extinction length for ice. Furthermore, in the absence of snow, the fraction of the net shortwave radiation that penetrates ice is taken to be 17% (Maykut & Untersteiner, 1971). In addition to the shortwave radiation, incoming longwave radiation, and specific and latent heat fluxes from the atmosphere, we also include a perturbation to the incoming longwave radiation, ΔF_0 , which represents the effects of additional greenhouse gas forcing.

Semtner's numerical formulation does not permit the inclusion of an internal heat source that represents the penetration of shortwave radiation (Semtner, 1976). Rather, this energy is stored in a "reservoir" and released during the fall freeze-up. The latent heat of fusion at the top surface is adjusted when the energy in the reservoir exceeds 30% of what is required to melt the entire ice layer (Semtner, 1976). When the thickness distribution is considered, this formulation makes the latent heat of fusion a function of the ice thickness, which is unphysical. Hence, we ignore this storage effect and note that it only impacts the time at which temperature of the upper ice surface drops below the freezing point in fall. We note here that neglecting brine pockets and this heat source in the ice has implications for energy conservation, especially for long-time simulations (Bitz & Lipscomb, 1999). The three-layer Semtner model employed here is adequate to represent the effects of the snow cover and the specific heat of sea ice for our purposes. However, we emphasize that it is simple to use other thermodynamic models in this framework as we have shown previously (Toppaladoddi & Wettlaufer, 2017).

4. Results

We solve Equation 7 numerically using a flux-conserving, fully implicit, finite-difference scheme, subject to boundary conditions (Equation 14) and $g(\infty) = 0$, or $g(0) = 0$ and $g(\infty) = 0$. The growth and decay of open water fraction is accompanied by the evolution of a boundary layer at $h = 0$, the resolution of which requires a finer numerical grid than in our previous work (Toppaladoddi & Wettlaufer, 2017). The radiative fluxes used to compute the growth rate are taken from observations (Maykut & Untersteiner, 1971). Finally, unless otherwise stated, ΔF_0 is set to 0 Wm^{-2} and F_B , the oceanic heat flux, is set to 2 Wm^{-2} .

The results presented in the following sections were obtained after the system reached a statistically steady state.

4.1. Seasonality of the Ice Thickness Distribution

We first focus on the evolution of $g(h)$ during a typical year. Figures 2a–2d show that during winter (summer), $g(h)$ expands (contracts), in agreement with observations (Kwok & Cunningham, 2015). The key features are as follows: (a) The distribution for June 15 in Figure 2C is double-peaked; (b) The value of the vertical

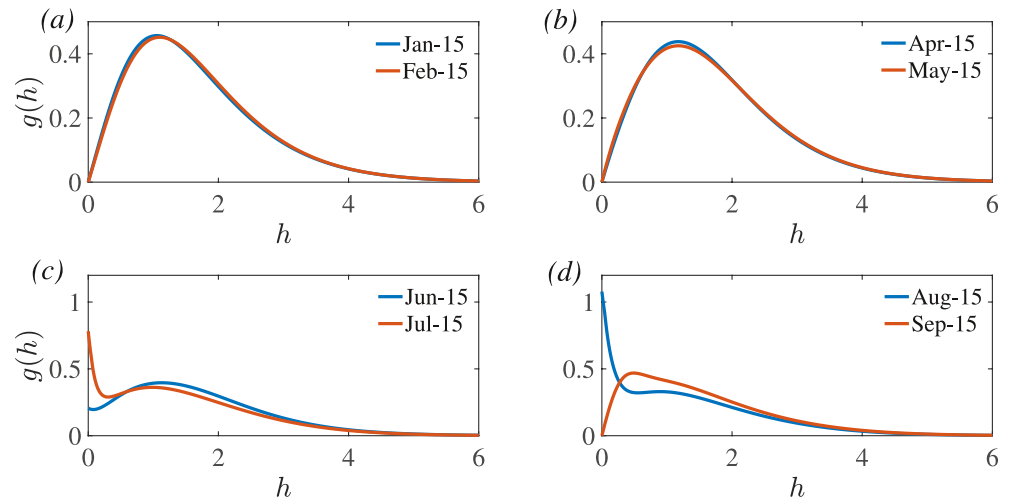


Figure 2. Thickness distributions during different months for $F_B = 2 \text{ Wm}^{-2}$ and $\Delta F_0 = 0$. The second peak in $g(h)$ emerges around June 15, which is seen in figure (c).

intercept, $g(0)$, increases from June to August, as seen in Figure 2d; and (c) as fall begins, this double-peaked distribution evolves to a single-peaked distribution in September, as shown in Figure 2d. These distributions should be contrasted with the those obtained by Toppaladoddi and Wettlaufer (2017) using $g(0) = 0$ for the entire season.

Of particular interest is the double-peaked $g(h)$ obtained here, which is a much sought after observational feature of the seasonal ice-pack. For example, similar profiles for the PDF of draft (the thickness of the submerged portion of sea ice) have been obtained using upward looking sonar measurements from submarines (Yu et al., 2004). These profiles have been converted to the sea-ice thickness and have been normalized. Figure 3 shows a qualitative comparison between $g(h)$ for July 15 obtained from theory and the $g(h)$ from submarine measurements from SCICEX cruises, which were made during September 1993 with the data averaged over the entire cruise track (Yu et al., 2004). The agreement between theory and observations is evident, with the timing of the onset of the second peak being controlled by the heat capacity of ice and the snow layer. The observations in Figure 3 can also be compared with the distribution on August 15 in Figure 2d, which shows a distinct second peak. Note that, relative to winter, the summer satellite sea-ice thickness record from CryoSat-2 has many sources of variability (Landy et al., 2022).

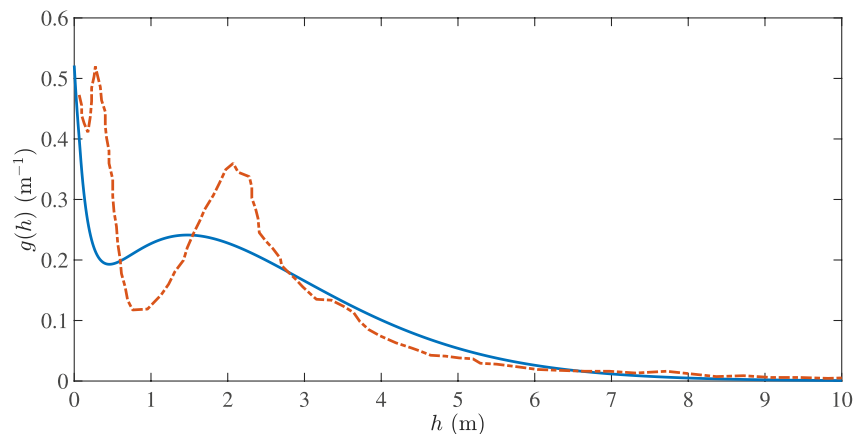


Figure 3. Qualitative comparison of doubled-peaked $g(h)$ with observations. The solid line represents $g(h)$ for July 15 obtained from theory, and the dashed line represents the $g(h)$ from SCICEX measurements in September 1993 averaged over the entire cruise track in the Arctic (Yu et al., 2004). The $g(h)$ from the theory has been made dimensional by scaling with H_{eq} , and the original distribution for draft from Yu et al. (2004) has been converted to that for thickness and normalized.

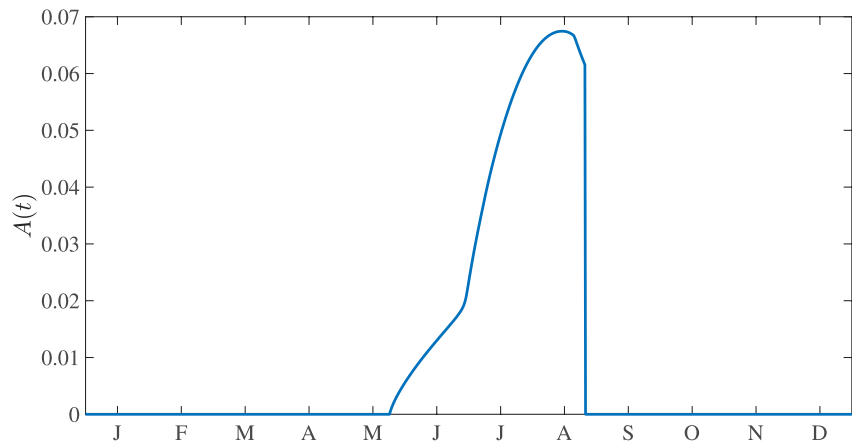


Figure 4. Evolution of $A(t)$ during a typical year for $F_B = 2 \text{ Wm}^{-2}$ and $\Delta F_0 = 0$.

4.2. Evolution of the Open-Water Fraction

The seasonal evolution of the open water fraction, $A(t)$, shown in Figure 4, constitutes a key aspect of the evolution of $g(h)$ shown in Figure 2. From the fall freeze-up through May the open water fraction is nearly zero, after which it starts to increase appreciably. The maximum value of A ($\approx 6.7\%$) is attained in mid-August. This qualitative behavior of $A(t)$ is clearly in accord with both intuition and, most importantly, large-scale observations in the Arctic (Kwok & Cunningham, 2015; Kwok et al., 2009).

4.3. Mean Thickness and Albedo

The mean of any thickness-dependent quantity, $\Phi(h)$, is given by

$$\langle \Phi(t) \rangle = \int_0^\infty \Phi(h) g(h, t) dh. \quad (16)$$

Using this relation we calculate $\langle h \rangle$ and $\langle \alpha \rangle$, whose seasonal cycles are shown in Figure 5 for $F_B = 2 \text{ Wm}^{-2}$ and $\Delta F_0 = 0$. Clearly $\langle h \rangle$ reaches a maximum ($\approx 1.74 \text{ m}$) in the last week of May and a minimum ($\approx 1.25 \text{ m}$) in the last week of August. These values are lower than for the case when $g(0) = 0$ is imposed as a boundary condition throughout the year (Toppaladoddi & Wettlaufer, 2017). A similar change can also be seen in $\langle \alpha \rangle$ which here varies between 0.668 in early April to 0.593 in mid-August. Note that $\langle \alpha \rangle$ leads $\langle h \rangle$, underlying the ice-albedo feedback.

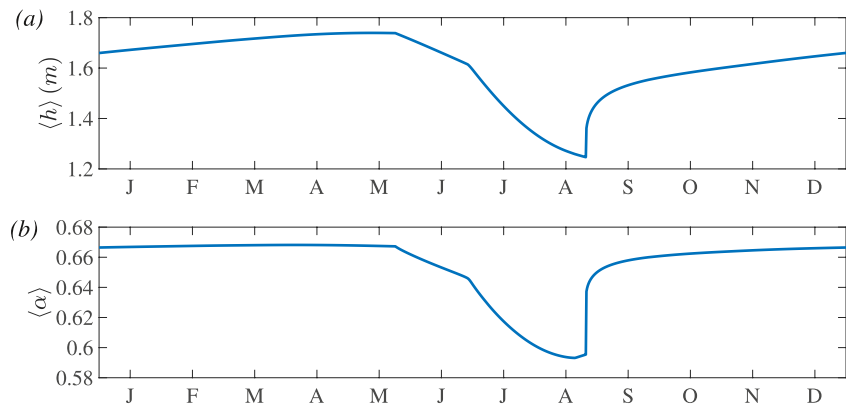


Figure 5. Evolution of (a) mean thickness, $\langle h \rangle$; and (b) mean albedo, $\langle \alpha \rangle$ for $F_B = 2 \text{ Wm}^{-2}$ and $\Delta F_0 = 0$.

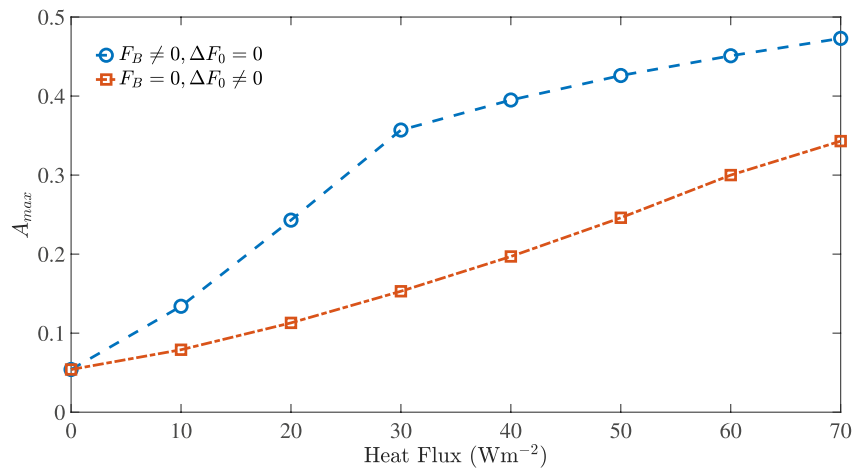


Figure 6. Changes in the maximum value of the open-water fraction, A_{\max} , with F_B and ΔF_0 .

4.4. Effects of Ocean Heat Flux and Greenhouse-Gas Forcing on the Open-Water Fraction and the Mean Thickness

Figure 6 shows the changes in the maximum value of open-water fraction, A_{\max} , for the different values of F_B and ΔF_0 . Two main features are apparent: First, an increase in the value of F_B and/or ΔF_0 leads to an increase in the value of A_{\max} . Second, the increase in A_{\max} due to F_B is more rapid than that for ΔF_0 . Thus the ice cover is more sensitive to the ice-ocean heat flux than it is to the greenhouse-gas forcing at the upper surface. This is due to the fact that in a thermodynamic model when the Stefan number is large the temperature gradient in the ice is quasi-steady and linear (Eisenman & Wettlaufer, 2009). Thus both ΔF_0 and F_B have the same impact on the ice thickness, whereas in a model with curvature in the temperature field these forcings are local. This sensitivity of the ice cover to the ocean heat flux is also in qualitative agreement with the results from the thermodynamic-only model of Maykut and Untersteiner (1971).

Not only do F_B and ΔF_0 impact the maximum values of $A(t)$, but also its minimum values and the time at which open water starts forming, as shown in Figure 7. When $\Delta F_0 = 25 \text{ Wm}^{-2}$ and $F_B = 0$, which corresponds to a six-fold increase in the CO_2 concentration in the atmosphere, open water begins to form near the middle of May and persists until early September. This is due to the fact that the increase in ΔF_0 leads to an earlier disappearance of the snow layer, and hence earlier melting of the ice layer. These changes can be clearly contrasted with the case when both ΔF_0 and F_B are set to zero. Importantly, we note that the choice of $\Delta F_0 = 25 \text{ Wm}^{-2}$ and $F_B = 0$ has been made to highlight the effects of these fluxes on the ice cover. Clearly, when there is a substantial increase in the atmospheric CO_2 concentration the oceanic heat flux will increase.

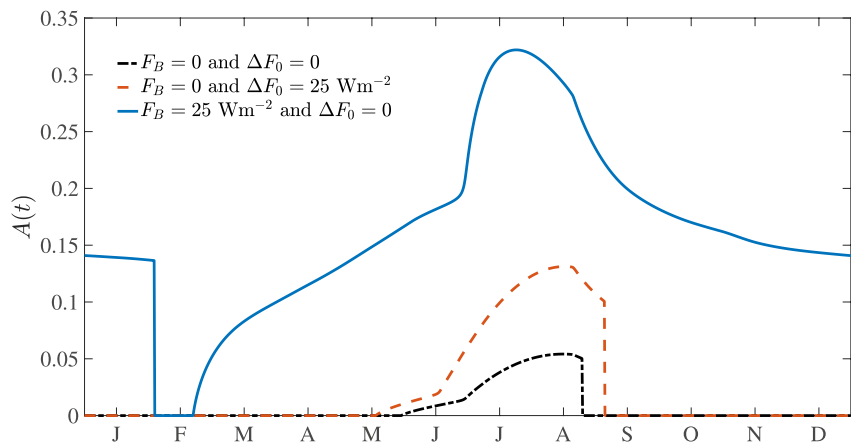


Figure 7. Changes in $A(t)$ for different values of F_B and ΔF_0 .

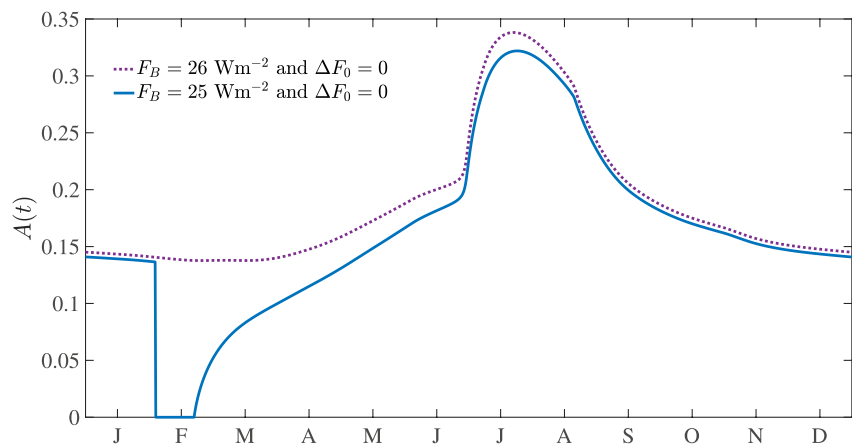


Figure 8. Changes in $A(t)$ for $F_B = 25$ and 26 Wm^{-2} .

The changes in $A(t)$ due to F_B are more striking. When $F_B = 25 \text{ Wm}^{-2}$ (and $\Delta F_0 = 0$), A_{max} is about 32%, and open water is present throughout nearly the entire year. Moreover, the change in the energy balance is such that thin ice only grows from open water during only 3 weeks in February. To further highlight the sensitivity of the ice cover to F_B , we show in Figure 8 the evolution of $A(t)$ for $F_B = 25$ and 26 Wm^{-2} . An increase in F_B of just 1 Wm^{-2} results in open water throughout the year. These effects are due to the thickest ice being ostensibly isothermal at the base and hence any non-zero value of F_B drives ablation (Maykut & Untersteiner, 1971). This leads to a greater thinning of the ice cover as shown in Figure 9.

Similar effects of F_B and ΔF_0 are also seen in the changes to the time-averaged mean thickness, $\overline{\langle h \rangle}$, which are shown in Figure 9. Here, the time average is taken over a typical year in the statistically steady state. The decay in $\overline{\langle h \rangle}$ with F_B is exponential, whereas it is algebraic with ΔF_0 . When $F_B = 60 \text{ Wm}^{-2}$, $\overline{\langle h \rangle} = 0.1 \text{ m} = H_c$, which implies that it is difficult to distinguish between thin ice and open water. The value of the basal heat flux for which nearly ice-free conditions are observed with $g(h)$ is an order of magnitude larger than seen in the calculations of Maykut and Untersteiner (1971), but is consistent with more recent measurements made in the Arctic (McPhee, 1992; Stanton et al., 2012; Wettlaufer, 1991). This persistence of the ice cover has two principal causes both captured by our theory: The thickest ice survives the melt season and thinner ice rafts and ridges to become thicker and hence has a higher albedo through Equation 15.

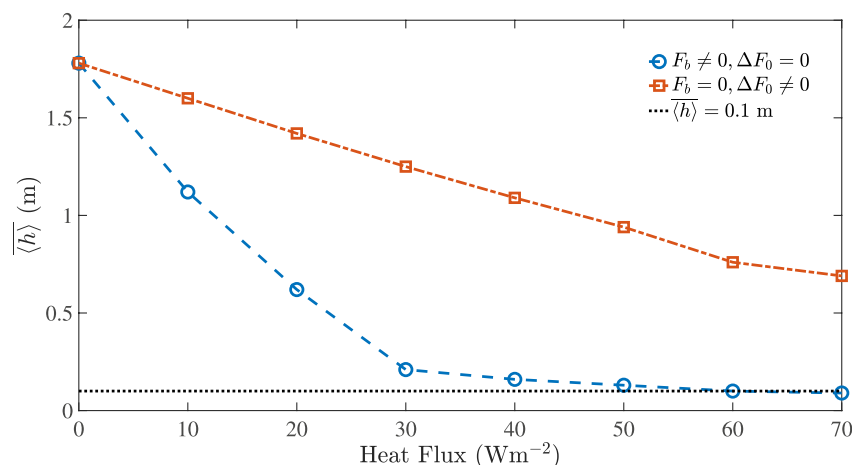


Figure 9. Changes in the time-averaged mean thickness, $\overline{\langle h \rangle}$, with F_B and ΔF_0 .

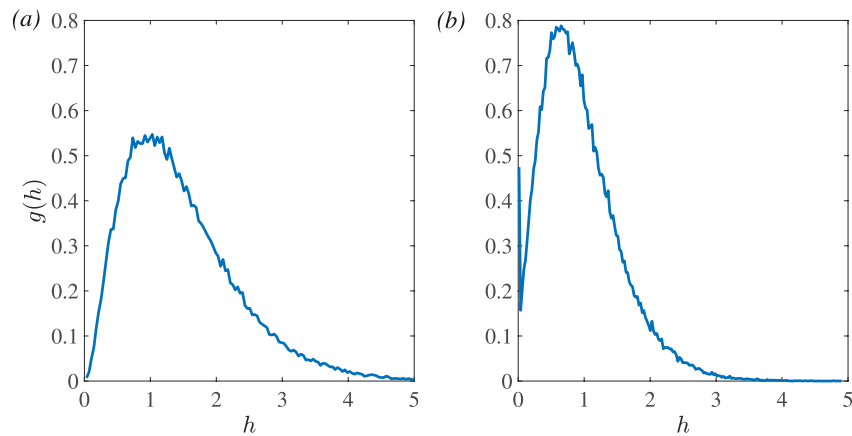


Figure 10. Distributions obtained from solving Equation 17 for $F_B = 5 \text{ Wm}^{-2}$ and $\Delta T = 5^\circ\text{C}$. Here, $N_{en} \approx 10^5$, $\mathcal{T} = 1.25$, and $\Delta t = 5 \times 10^{-5}$. Figure (a) shows the initial $g(h)$ and figure (b) shows the $g(h)$ at the end of integration.

4.5. Transition From a Single- to a Double-Peaked Distribution

To examine the transition of $g(h)$ from being single- to double-peaked, we use the equivalent Langevin formulation corresponding to Equation 7, which is

$$\frac{dh}{dt} = (\tau f - k_1) + \sqrt{2k_2} \xi(t), \quad (17)$$

where $(\tau f - k_1)$ and $\sqrt{2k_2} \xi(t)$ are the drift and diffusion terms, respectively, and $\xi(t)$ is Gaussian white noise (Toppaladoddi & Wettlaufer, 2015). The growth rate here is taken to be

$$f = \frac{1}{\rho_i L_i f_0} \left(k_i \frac{\Delta T}{h} - F_B \right), \quad (18)$$

where k_i is the thermal conductivity of ice, ΔT is the temperature difference across the ice layer, and, as we have done throughout, we assume F_B to be a constant.

An ensemble of $N_{en} \approx 10^5$ thicknesses constitute the initial conditions for Equation 17, such that their distribution corresponds to the winter solution of Equation 9. For each realization Equation 17 is then integrated for $\mathcal{T} = 1.25$ in non-dimensional units. The behavior at the origin is treated by requiring that if $h < 0$ at the end of integration in any realization, then h is set to 0.

The transition in $g(h)$ to a double-peaked distribution is shown in Figure 10. Clearly, as the energy balance on the right hand side of Equation 18 changes, so too does the sign of the drift term in Equation 17. Therefore, the principal factor responsible for the emergence of the double-peaked distribution is the change in energy balance.

5. Conclusions

We have closed the original theory of the sea ice thickness distribution of Thorndike et al. (1975) by recasting the mechanical redistribution function in terms of the probability density of ice thickness itself; $g(h)$. In consequence of this closure the original theory becomes a Fokker-Planck equation. We then generalized the theory to include the seasonal variation in the open water fraction. This is achieved by formulating a new boundary condition for $g(h)$ at $h = 0$. The numerical solutions show a transition from a single-peaked to a double-peaked $g(h)$ in summer, in general agreement with submarine measurements from SCICEX cruises made in 1993 (Yu et al., 2004).

Our formulation makes the explicit calculation of the open-water fraction, $A(t)$, possible. In the absence of excess greenhouse-gas forcing, $\Delta F_0 = 0$, the solutions reveal that $A(t) \approx 0$ during the winter months, increases near the end of May and persists until the end of August. However, an increase in ΔF_0 to 25 Wm^{-2} shifts the onset of open-water formation to the middle of May and it persists until early September.

Particularly dramatic are the effects of the basal heat flux, F_B , on the ice cover. The time-averaged mean thickness decreases exponentially with increasing F_B , and when $F_B = 26 \text{ Wm}^{-2}$, open water persists for the

entire year. However, the value of F_b for which nearly ice-free conditions are observed with $g(h)$ is an order of magnitude larger than seen in the thermodynamic-only calculations (Eisenman & Wettlaufer, 2009; Maykut & Untersteiner, 1971; Semtner, 1976). This is because in our theory for $g(h)$ the thickest ice survives the melt season and thinner ice rafts and ridges to become thicker and hence has a higher albedo. The basal heat flux is thus far more impactful than is greenhouse-gas forcing, ΔF_0 .

These results also highlight the different roles played by thermodynamics and mechanics in the evolution of the ice cover as the Arctic ocean warms (Timmermans, 2015; Timmermans et al., 2018). An increase in the ocean heat flux tends to make the ice cover thinner, but the mechanical redistribution of ice prolongs its survival.

The necessity of including the thickness distribution into global and regional climate models to accurately capture the atmosphere-ice-ocean interactions has long been recognized in the sea-ice modeling community (Bitz et al., 2001; Hibler, 1979; Smith et al., 2022). The thickness distribution is generally resolved using five thickness categories (excluding open water) and the treatment of the mechanical redistribution is based on the original formulation of Thorndike et al. (1975), which—according to Thorndike et al. (1975)—is “arbitrary.” The principal source of this arbitrariness comes from the need to specify the range of ice thicknesses on the thin end of the thickness distribution that ridge to form thicker ice. However, in principle, ice of all thicknesses can participate in ridging (Vella & Wettlaufer, 2008).

The inclusion of the thickness distribution is crucial for improving the energy balance in climate models. However, the arbitrariness associated with the mechanical redistribution of sea ice is a possible reason why some climate models include a thickness distribution that does not evolve in time (Castro-Morales et al., 2014). Indeed, despite advances in sea-ice modeling, the Coupled Model Intercomparison Project models do not realistically capture the observed spatial distribution of sea ice thickness or ice extent (Agarwal & Wettlaufer, 2018; Stroeve et al., 2014; Wei et al., 2020). Hence, we believe that progress can be made by addressing the issue of the arbitrariness associated with the mechanical redistribution of sea ice.

Our theory does not suffer from this arbitrariness and allows for mechanical interactions in ice of any thickness. We show that the theory provides a physically robust and observationally consistent framework to study the seasonal evolution of the thickness distribution. Moreover, our prediction of the emergence of a second peak in the distribution, which is a key aspect of observations, highlights the necessity of the higher resolution required to capture the behavior near $h = 0$ in summer (Figure 3a). Finally, it is hoped that our work will lead to a more realistic representation of the thickness distribution in climate models, and hence to more accurate predictions of the fate of the Arctic ice cover.

Data Availability Statement

All the data are available within the manuscript. The numerical code used to solve the Fokker-Planck equation is available at <https://github.com/skleeds23/Thickness-distribution-of-sea-ice.git>. The satellite data used in Figure 1 were extracted from the plot for $g(h)$ in Figure 6e in Kwok et al. (2009).

Acknowledgments

The authors acknowledge the support of the Universities of Leeds and Oxford, NORDITA, and Yale University. S.T. acknowledges a Research Fellowship from All Souls College, Oxford and helpful discussions with A. J. Wells. W.M. and J.S.W. acknowledge Swedish Research Council Grant 638-2013-9243 for support. Nordita is partially supported by Nordforsk.

References

- Agarwal, S., & Wettlaufer, J. S. (2017). The statistical properties of sea ice velocity fields. *Journal of Climate*, 30(13), 4873–4881. <https://doi.org/10.1175/jcli-d-16-0653.1>
- Agarwal, S., & Wettlaufer, J. S. (2018). Fluctuations in Arctic sea-ice extent: Comparing observations and climate models. *Philosophical Transactions of the Royal Society A*, 376(2129), 20170332. <https://doi.org/10.1098/rsta.2017.0332>
- Bitz, C. M., Holland, M. M., Weaver, A. J., & Eby, M. (2001). Simulating the ice-thickness distribution in a coupled climate model. *Journal of Geophysical Research*, 106(C2), 2441–2463. <https://doi.org/10.1029/1999jc000113>
- Bitz, C. M., & Lipscomb, W. H. (1999). An energy-conserving thermodynamic model of sea ice. *Journal of Geophysical Research*, 104(C7), 15669–15677. <https://doi.org/10.1029/1999jc900100>
- Castro-Morales, K., Kauker, F., Losch, M., Hendricks, S., Riemann-Campe, K., & Gerdes, R. (2014). Sensitivity of simulated Arctic sea ice to realistic ice thickness distributions and snow parameterizations. *Journal of Geophysical Research: Oceans*, 119(1), 559–571. <https://doi.org/10.1002/2013jc009342>
- Coon, M., Kwok, R., Levy, G., Pruis, M., Schreyer, H., & Sulsky, D. (2007). Arctic Ice Dynamics Joint Experiment (AIDJEX) assumptions revisited and found inadequate. *Journal of Geophysical Research*, 112(C11), C11S90. <https://doi.org/10.1029/2005JC003393>
- Courant, R., & Hilbert, D. (1953). *Methods of mathematical physics* (Vol. II). Interscience.
- Eisenman, I., & Wettlaufer, J. S. (2009). Nonlinear threshold behavior during the loss of Arctic sea ice. *Proceedings of the National Academy of Sciences*, 106(1), 28–32. <https://doi.org/10.1073/pnas.0806887106>
- Feltham, D. L. (2008). Seaicerheology. *Annual Review of Fluid Mechanics*, 40(1), 91–112. <https://doi.org/10.1146/annurev.fluid.40.1.11406.102151>

- Godlovitch, D., Illner, R., & Monahan, A. (2011). Smoluchowski coagulation models of sea ice thickness distribution dynamics. *Journal of Geophysical Research*, *116*(C12), C12005. <https://doi.org/10.1029/2011jc007125>
- Hibler, W. D., III. (1979). A dynamic thermodynamic sea ice model. *Journal of Physical Oceanography*, *9*(4), 815–846. [https://doi.org/10.1175/1520-0485\(1979\)009<0815:adtsim>2.0.co;2](https://doi.org/10.1175/1520-0485(1979)009<0815:adtsim>2.0.co;2)
- Horvat, C., & Tziperman, E. (2015). A prognostic model of the sea-ice floe size and thickness distribution. *The Cryosphere*, *9*(6), 2119–2134. <https://doi.org/10.5194/tc-9-2119-2015>
- Kwok, R., & Cunningham, G. (2015). Variability of Arctic sea ice thickness and volume from CryoSat-2. *Philosophical Transactions of the Royal Society A*, *373*(2045), 20140157. <https://doi.org/10.1098/rsta.2014.0157>
- Kwok, R., Cunningham, G., Wensnahan, M., Rigor, I., Zwally, H., & Yi, D. (2009). Thinning and volume loss of the Arctic Ocean sea ice cover: 2003–2008. *Journal of Geophysical Research*, *114*(C7), C07005. <https://doi.org/10.1029/2009jc005312>
- Kwok, R., Petty, A. A., Bagnardi, M., Kurtz, N. T., Cunningham, G. F., Ivanoff, A., et al. (2021). Refining the sea surface identification approach for determining freeboards in the ICESat-2 sea ice products. *The Cryosphere*, *15*(2), 821–833. <https://doi.org/10.5194/tc-15-821-2021>
- Kwok, R., & Untersteiner, N. (2011). The thinning of Arctic sea ice. *Physics Today*, *64*(4), 36–41. <https://doi.org/10.1063/1.3580491>
- Landy, J. C., Dawson, G. J., Tsamados, M., Bushuk, M., Stroeve, J. C., Howell, S. E. L., et al. (2022). A year-round satellite sea-ice thickness record from CryoSat-2. *Nature*, *609*(7927), 517–522. <https://doi.org/10.1038/s41586-022-05058-5>
- Manabe, S., & Wetherald, R. T. (1975). The effects of doubling the CO₂ concentration on the climate of a general circulation model. *Journal of the Atmospheric Sciences*, *32*(1), 3–15. [https://doi.org/10.1175/1520-0469\(1975\)032<0003:teodtc>2.0.co;2](https://doi.org/10.1175/1520-0469(1975)032<0003:teodtc>2.0.co;2)
- Maykut, G. A., & Untersteiner, N. (1971). Some results from a time-dependent thermodynamic model of sea ice. *Journal of Geophysical Research*, *76*(6), 1550–1575. <https://doi.org/10.1029/jc076i006p01550>
- McPhee, M. G. (1992). Turbulent heat flux in the upper ocean under sea ice. *Journal of Geophysical Research*, *97*(C4), 5365–5379. <https://doi.org/10.1029/92jc00239>
- Pawula, R. F. (1967). Approximation of the linear Boltzmann equation by the Fokker–Planck equation. *Physical Review*, *162*(1), 186–188. <https://doi.org/10.1103/physrev.162.186>
- Roberts, A. F., Hunke, E. C., Kamal, S. M., Lipscomb, W. H., Horvat, C., & Maslowski, W. (2019). A variational method for sea ice ridging in Earth system models. *Journal of Advances in Modeling Earth Systems*, *11*(3), 771–805. <https://doi.org/10.1029/2018MS001395>
- Rothrock, D. A. (1975). The mechanical behaviour of pack ice. *Annual Review of Earth and Planetary Sciences*, *3*(1), 317–342. <https://doi.org/10.1146/annurev.ea.03.050175.001533>
- Rothrock, D. A., & Thorndike, A. S. (1980). Geometric properties of the underside of the sea ice. *Journal of Geophysical Research*, *85*(C7), 3955–3963. <https://doi.org/10.1029/jc085ic07p03955>
- Rothrock, D. A., & Thorndike, A. S. (1984). Measuring the sea ice floe size distribution. *Journal of Geophysical Research*, *89*(NC4), 6477–6486. <https://doi.org/10.1029/jc089ic04p06477>
- Semtner, A. J. (1976). A model for the thermodynamic growth of sea ice in numerical investigations of climate. *Journal of Physical Oceanography*, *6*(3), 379–389. [https://doi.org/10.1175/1520-0485\(1976\)006<0379:amftg>2.0.co;2](https://doi.org/10.1175/1520-0485(1976)006<0379:amftg>2.0.co;2)
- Smith, M. M., Holland, M. M., Petty, A. A., Light, B., & Bailey, D. A. (2022). Effects of increasing the category resolution of the sea ice thickness distribution in a coupled climate model on Arctic and Antarctic sea ice mean state. *Journal of Geophysical Research: Oceans*, *127*(10), e2022JC019044. <https://doi.org/10.1029/2022jc019044>
- Stanton, T. P., Shaw, W. J., & Hutchings, J. K. (2012). Observational study of relationships between incoming radiation, open water fraction, and ocean-to-ice heat flux in the transpolar drift: 2002–2010. *Journal of Geophysical Research*, *117*(C7). <https://doi.org/10.1029/2011jc007871>
- Stroeve, J., Barrett, A., Serreze, M., & Schweiger, A. (2014). Using records from submarine, aircraft and satellites to evaluate climate model simulations of Arctic sea ice thickness. *The Cryosphere*, *8*(5), 1839–1854. <https://doi.org/10.5194/tc-8-1839-2014>
- Thorndike, A. S. (1992). Estimates of sea ice thickness distribution using observations and theory. *Journal of Geophysical Research*, *97*(C8), 12601–12605. <https://doi.org/10.1029/92jc01199>
- Thorndike, A. S. (2000). Sea ice thickness as a stochastic process. *Journal of Geophysical Research*, *105*(C1), 1311–1313. <https://doi.org/10.1029/1999jc900271>
- Thorndike, A. S., Rothrock, D. A., Maykut, G. A., & Colony, R. (1975). Thickness distribution of sea ice. *Journal of Geophysical Research*, *80*(33), 4501–4513. <https://doi.org/10.1029/jc080i033p04501>
- Timmermans, M.-L. (2015). The impact of stored solar heat on Arctic sea ice growth. *Geophysical Research Letters*, *42*(15), 6399–6406. <https://doi.org/10.1002/2015gl064541>
- Timmermans, M.-L., Toole, J., & Krishfield, R. (2018). Warming of the interior Arctic Ocean linked to sea ice losses at the basin margins. *Science Advances*, *4*(8), eaat6773. <https://doi.org/10.1126/sciadv.aat6773>
- Toppaladoddi, S., & Wettlaufer, J. S. (2015). Theory of the sea ice thickness distribution. *Physical Review Letters*, *115*(14), 148501. <https://doi.org/10.1103/physrevlett.115.148501>
- Toppaladoddi, S., & Wettlaufer, J. S. (2017). Statistical mechanics and the climatology of the Arctic Sea ice thickness distribution. *Journal of Statistical Physics*, *167*(3–4), 683–702. <https://doi.org/10.1007/s10955-016-1704-8>
- Untersteiner, N., Thorndike, A. S., Rothrock, D. A., & Hunkins, K. L. (2007). AIDJEX revisited: A look back at the US-Canadian Arctic ice dynamics joint experiment 1970–78. *Arctic*, *60*(3), 327–336. <https://doi.org/10.14430/arctic233>
- Vella, D., & Wettlaufer, J. S. (2008). Explaining the patterns formed by ice floe interactions. *Journal of Geophysical Research*, *113*(C11), C11011. <https://doi.org/10.1029/2008jc004781>
- Wei, T., Yan, Q., Qi, W., Ding, M., & Wang, C. (2020). Projections of Arctic sea ice conditions and shipping routes in the twenty-first century using CMIP6 forcing scenarios. *Environmental Research Letters*, *15*(10), 104079. <https://doi.org/10.1088/1748-9326/abb2c8>
- Wettlaufer, J. S. (1991). Heat flux at the ice-ocean interface. *Journal of Geophysical Research*, *96*(C4), 7215–7236. <https://doi.org/10.1029/90jc00081>
- Yu, Y., Maykut, G., & Rothrock, D. (2004). Changes in the thickness distribution of Arctic sea ice between 1958–1970 and 1993–1997. *Journal of Geophysical Research*, *109*(C8). <https://doi.org/10.1029/2003jc001982>